

# NJC

Accepted Manuscript



This is an *Accepted Manuscript*, which has been through the Royal Society of Chemistry peer review process and has been accepted for publication.

*Accepted Manuscripts* are published online shortly after acceptance, before technical editing, formatting and proof reading. Using this free service, authors can make their results available to the community, in citable form, before we publish the edited article. We will replace this *Accepted Manuscript* with the edited and formatted *Advance Article* as soon as it is available.

You can find more information about *Accepted Manuscripts* in the [Information for Authors](#).

Please note that technical editing may introduce minor changes to the text and/or graphics, which may alter content. The journal's standard [Terms & Conditions](#) and the [Ethical guidelines](#) still apply. In no event shall the Royal Society of Chemistry be held responsible for any errors or omissions in this *Accepted Manuscript* or any consequences arising from the use of any information it contains.

# Optical Properties of two fluorene derived BODIPY molecular rotors as fluorescent ratiometric viscosity probes

Elba Xochitiotzi-Flores,<sup>a,‡</sup> Arturo Jiménez-Sánchez,<sup>b,‡</sup> Héctor García-Ortega,<sup>a</sup> Nuria Sanchez-Puig,<sup>c</sup> Margarita Romero-Ávila,<sup>a</sup> Rosa Santillan,<sup>d</sup> Norberto Farfán<sup>a,\*</sup>

## Abstract

BODIPY-derived molecular fluorescent rotors are one of the most useful families of fluorescent probes for quantitative measurement of microviscosity. Here, we report on the photophysical properties of two molecular rotors as ratiometric viscosity sensors, *meso*-(4-(9*H*-fluoren-2-yl)ethynyl)phenyl-4,4-difluoro-4-bora-3a,4a-diaza-*s*-indacene (**1**) and *meso*-(5-(9*H*-fluoren-2-yl)ethynyl)thiophen-2-yl-4,4-difluoro-4-bora-3a,4a-diaza-*s*-indacene (**2**) having two independent chromophores, one of them (Fluorene) is not influenced by viscosity and is used to determine concentration properties, and the other chromophore (BODIPY) acts as a molecular rotor. The fluorescence ratiometric calibration against microviscosity for most sensitive probe **1**, was obtained in a wide linear dynamic range. The sensitivity of the spectroscopic observables for **1** and **2** towards solvent viscosity and the typical analytical interfering solvent polarity and polarizability parameters was investigated by means of two different solvent scales, namely Lippert-Mataga and Catalán finding consistent results. Quantum chemical calculations were conducted to analyze the probe mechanism in terms of Natural Transition Orbitals (NTOs) and spatial extent of charge transfer excitations.

**Keywords:** Fluorene, BODIPY, Fluorescent Viscosity Sensors, Förster-Hoffmann relation, fluorescent molecular rotor.

## 1. Introduction

Macro-/micro-environment sensing has become an interesting research area since local environment is by far the most relevant factor governing the physical and chemical behavior of surrounding molecules.<sup>1</sup> The fluorescence sensing of viscosity, polarity, polarizability, local acidity/basicity, pH and temperature has significantly contributed to

define specific location properties.<sup>2</sup> In this respect, viscosity plays paramount roles in diffusion-controlled processes like cellular transport in membrane systems.<sup>3</sup>

Within the broad range of compounds designed for the fluorescent recognition of viscosity, the *p*-amino-benzylidene malononitriles represent a family of compounds typically used for these purposes.<sup>2,4</sup> This is due to their molecular rotor characteristics that enable molecules to undergo a twist-intramolecular charge transfer process (TICT) in the excited state.<sup>5</sup> However, unlike the most studied D- $\pi$ -A fluorophores, fluorene-BODIPY D- $\pi$ -A systems constitute a promising and interesting family of compounds with excellent spectroscopic properties like modular Stokes Shifts, high photochemical stability, relatively high absorption coefficients and narrow absorption and emission bands,<sup>6</sup> and most importantly, their narrow emission band allows a well separated  $\lambda$ -ratiometric response to enable a complete band differentiation.

On the other hand, ratiometric or  $\lambda$ -ratiometric fluorescence sensing<sup>7a</sup> is a highly valuable method since simple fluorescence intensity-based sensing depends on the power of excitation, on the sensitivity of the detector and on the calibration/correction of the fluorescence response.<sup>8</sup> Thus, to overcome such limitations, a ratio between two bands in the dual-fluorescence spectrum of this fluorescent probes can be utilized. Regarding the viscosity,  $\lambda$ -ratiometry measurements are required when both, the intensity and the emission wavelength change as a result of intermolecular interactions of a specific part of the fluorophore with the local environment.<sup>8</sup>

In this work, we describe two novel ethynyl-fluorene derived BODIPY probes as highly sensitive fluorescent viscosity sensors. Firstly, we describe the synthesis and characterization of *meso*-(4-(9*H*-fluoren-2-yl)ethynyl)phenyl-4,4-difluoro-4-bora-3a,4a-diaza-*s*-indacene (**1**) and *meso*-(5-(9*H*-fluoren-2-yl)ethynyl)thiophen-2-yl-4,4-difluoro-4-bora-3a,4a-diaza-*s*-indacene (**2**). Then, the UV-Vis absorption and fluorescence properties were investigated to establish the relationship between fluorescence emission and solvent viscosity, polarity and polarizability parameters for **1** and **2**. Further, in terms of quantum chemical calculations, we provide a detailed description of the electronic properties of **1-2** in the frame of hole-electron interactions. Finally, we analyze the results by the evaluation of the charge transfer efficiency in terms of the spatial extent of the charge-transfer excitations.

## 2. Results and discussion

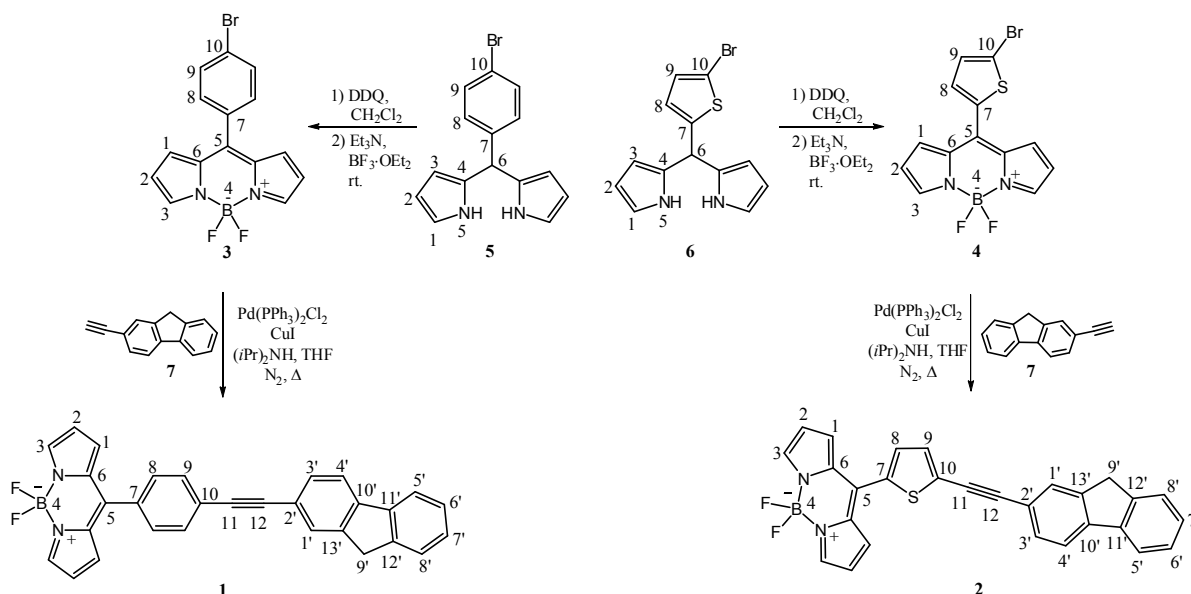
### 2.1. Design considerations for the ratiometric probes.

From the standpoint of electronic structure, the designed fluorene-BODIPY probes are in line with a Donor- $\pi$ -Acceptor array (D- $\pi$ -A, D = Fluorene,  $\pi$  = ethynylbenzene or ethynylthiophene, A = BODIPY), where the substitution pattern in the  $\pi$ -bridge leads to a linear dipolar system in compound **1**, whereas compound **2** adopts a “V-shaped” due to the 2,5-thiophene connector, allowing the system to experience a different amount of intramolecular charge transfer (ICT) process, making the probes sensitive to the local polarity of surrounding solvent molecules.<sup>9</sup> This represents a tremendously difficult problem for the design of BODIPY microviscosity probes, since as is well established, the boradiazaindacene subunit is electron deficient in nature and BODIPY substituents need to be connected through  $\pi$ -conjugated fragments having electron-donating features. In turn, fluorene is a well-known electron donor fluorophore.<sup>10</sup> To solve this problem, we utilized a conjugation length-elongation strategy by introducing a triple bond linkage between fluorene and 5-aryl-BODIPY moieties, which resulted highly efficient in inhibiting the ICT process, according to the theoretical computations of spatial extent of charge transfer excitations and solvatochromic analyses (see sections below). Very few examples of such a polarity independent ratiometric BODIPY microviscosity sensor exist,<sup>11</sup> however, this represents an exceptional advantage for two reasons: first, the fluorescence emission intensity is highly affected by both, solvent viscosity and solvent polarity, making impossible to perform a correct calibration of the rotor. Second, the bathochromic shift of fluorescence is caused either by an increase in solvent polarity due to ICT process or in the specific case of the TICT family of molecular probes.<sup>12</sup> These two disadvantages mean that the probe cannot be used in media of varied polarity, even for ratiometric approaches since both single and dual-emission bands are affected by solvent polarity in a different way. The same issues apply for solvent acidity and basicity parameters. Although, we think that ICT process is possible for compounds **1** and **2**.

### 2.2. Synthesis and Characterization of probes **1** and **2**

The BODIPYs *meso*-(4-(9*H*-fluoren-2-yl)ethynyl)phenyl-4,4-difluoro-4-bora-3a,4a-diaza-*s*-indacene **1** and *meso*-(5-(9*H*-fluoren-2-yl)ethynyl)-2-thiophenyl-4,4-difluoro-4-bora-3a,4a-diaza-*s*-indacene **2** were prepared by the synthetic route shown in Scheme 1. The corresponding aromatic aldehyde and six equivalents of pyrrole in the presence of a catalytic amount of CF<sub>3</sub>COOH were stirred at room temperature for 30 min to generate the corresponding dipyrromethane (**5**, **6**).<sup>13</sup> The isolation of the products was achieved by flash silica column chromatography and good yields were obtained for both compounds. In the next step the dipyrromethanes **5** and **6** were dissolved in anhydrous CH<sub>2</sub>Cl<sub>2</sub> and DDQ was added, the reaction was stirred for 30 min, then Et<sub>3</sub>N was added and the resulting solution was stirred for another 10 min, finally BF<sub>3</sub>·Et<sub>2</sub>O was added and the reaction was stirred overnight at room temperature. To isolate each compound, the crude reaction product was supported on celite and purified by flash chromatography. Following this procedure we were able to isolate the *meso*-(4-bromophenyl)-4,4-difluoro-4-bora-3a,4a-diaza-*s*-indacene **3**,<sup>14</sup> and *meso*-(5-bromothiophen-2-yl)-4,4-difluoro-4-bora-3a,4a-diaza-*s*-indacene **4** in 67% and 73% yield, respectively.

For the synthesis of 2-ethynyl-9*H*-fluorene **7**, we used 2-bromo-9*H*-fluorene and ethynyltrimethylsilane as starting materials with a Sonogashira cross-coupling reaction using Pd(PPh<sub>3</sub>)<sub>2</sub>Cl<sub>2</sub>/CuI and DIPA in anhydrous THF under nitrogen atmosphere. The reaction was stirred at 40 °C overnight and purification by flash chromatography resulted in the desired coupled product.



**Scheme 1.** Synthetic route of BODIPYs **1** and **2**.

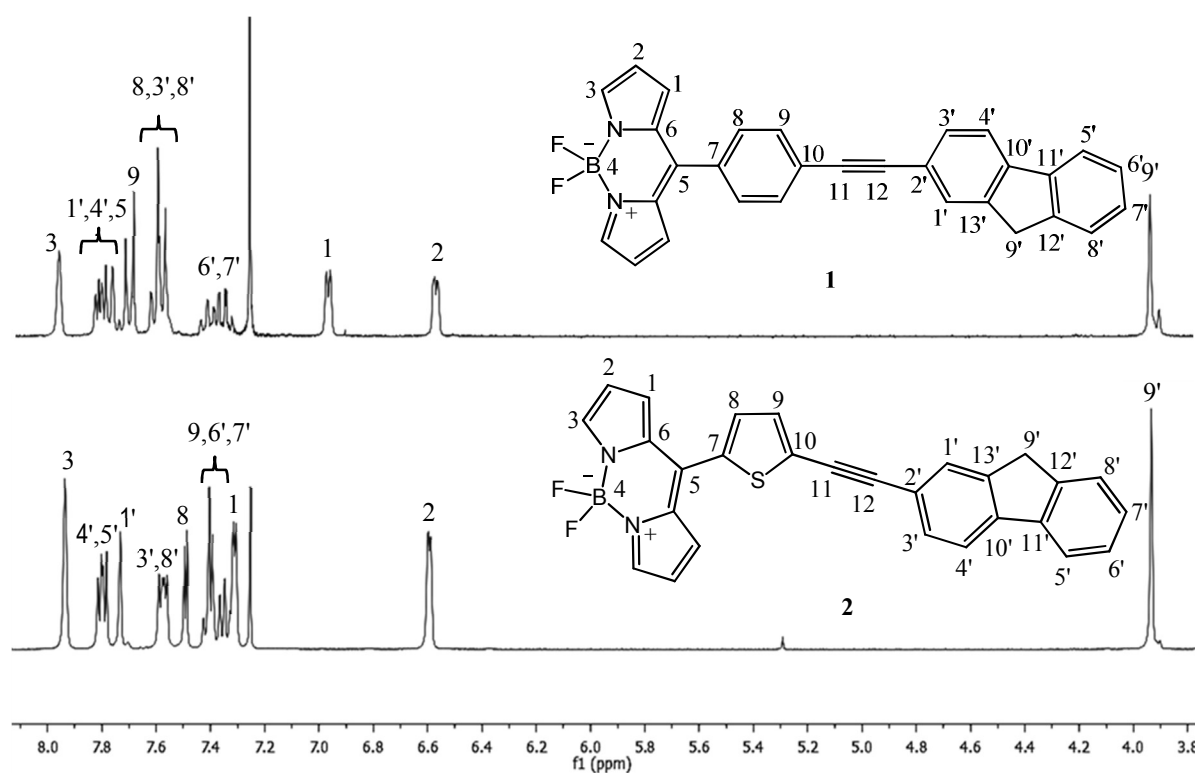


**Figure 1.** Comparison of <sup>1</sup>H NMR spectra of compounds **1** and **2** in CDCl<sub>3</sub>.

The isolated products were deprotected with K<sub>2</sub>CO<sub>3</sub>/methanol to generate compound **7** in 88% yield. Finally a second cross-coupling reaction using the conditions

mentioned above was carried out between the BODIPYs **3** or **4** and **7**, leading to the formation of two new BODIPYs **1** and **2**. The isolation of each product was performed by flash chromatography; the desired products were obtained in 70 and 63% yield, respectively.

The BODIPYs **1** and **2** are soluble in common organic solvents. The compounds **1-4** were characterized by spectroscopic techniques such as  $^1\text{H}$ ,  $^{13}\text{C}$  NMR, IR, absorption, fluorescence and HR-MS. Figure 1 shows the  $^1\text{H}$  NMR spectra of compounds **1** and **2**, we note the presence of signals corresponding to the starting BODIPYs at 7.96 and 7.94 ppm respectively, these appear as broad simple signals generated by the hydrogens adjacent to the nitrogen (H-3), as well as two signals at 6.97 and 7.31 (H-1), 6.58 and 6.59 (H-2) respectively. At low frequency are the expected signals corresponding to the methylene group of fluorene at 3.95 and 3.93 ppm, the other aromatic protons of **1** and **2** appear as expected between 7.35-7.82 and 7.35-7.81 ppm, respectively. The IR spectrum of **1** and **2** shows the corresponding band at 2201 and 2197  $\text{cm}^{-1}$  due to the  $\text{C}\equiv\text{C}$  stretching vibrations which confirms the presence of the BODIPY moiety. Complete characterization is presented in the ESI file, Figures S1-S8†.

### 2.3. UV-Vis and Fluorescence properties

The BODIPYs **1-4** were studied by absorption and fluorescence techniques. Comparison of the absorption spectra of these compounds is shown in Figure 2A and Table 1. Compounds **2-3** show the typical narrowed absorption band around 500 nm in chloroform, while compound **1** exhibits a blue-shifting of this band to 482 nm. This band is assigned to the 0-0 vibrational band of the  $\text{S}_0\rightarrow\text{S}_1$  electronic transition. In addition, a shoulder at higher energy corresponding to the 0-1 vibrational band of the same transition is observed for all the compounds. It is worth mentioning that a strong band widening is observed for **1**. The full width at half height of the maximum (fwhm) absorption band increases from 2440  $\text{cm}^{-1}$  in **2** to 4140  $\text{cm}^{-1}$  in **1**. Here is important to notice that a strong band broadening is obtained in chloroform, which can be attributed to partial aggregate formation, however, this is not observed for other solvents.

In the case of the fluorescence emission spectra, the substitution with ethynylfluorene provoked a strong fluorescence intensity decrease. The latter can be attributed to the charge

transfer deactivation channel.<sup>8</sup> On the other hand, the fluorene fragment fluorescence experiences a small intensity change (Figure 2B). Also, compound **3** exhibits a small Stokes shift which probably reflects the rigidity of the molecule in this media. However, probe **2** exhibits a new broad emission band red-shifted at 625 nm having no typical emissive BODIPY feature. In contrast, probe **1** has no fluorescence other than the fluorene emission band. Interestingly, a red-shifted emission band in **1** was observed only in the highly viscous monoethylene glycol (MEG) and propylene glycol (PG) solvents, from 16 tested solvents of different polarity/polarizability properties. This strong viscosity effect was further analyzed. Figure 3, in the next section, shows the fluorescence spectra of **1** and **2** in solvents with different viscosity but similar polarity properties. Further, Figure 4 and Table 2 show the solvatochromic analysis in 16 solvents and Figure S9† shows the excitation spectra corresponding to the long and short wavelength emission bands as well as the obtained fluorescence emission exciting at the long wavelength band.

**Table 1.** UV-Vis absorption and emission data for **1-4**.

Compound	$\lambda_{\text{max}}$ (Abs) [nm]	$\epsilon_{\text{max}}$ [dm <sup>3</sup> mol <sup>-1</sup> cm <sup>-1</sup> ]	$\lambda_{\text{max}}$ (Em) [nm]
<b>1</b>	476	25000	364
<b>2</b>	516	34000	382
<b>3</b>	504	49330	526
<b>4</b>	516	29330	630

<sup>a</sup> Concentration  $3.0 \times 10^{-5}$  M in chloroform.



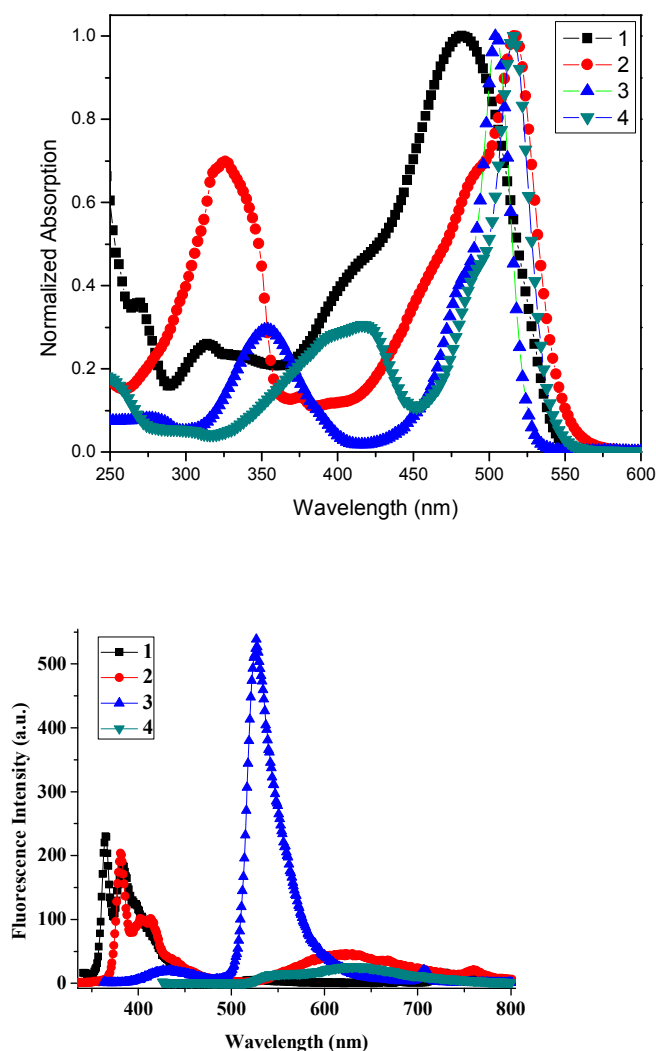


**Figure 2.** Comparison of absorption (above) and fluorescence (below,  $\lambda_{\text{ex}} = 330 \text{ nm}$ ) spectra of  $30 \mu\text{M}$  **1-4** recorded in  $\text{CHCl}_3$ .

#### 2.4. Viscosity vs. sensitivity in the fluorescence emission of **1-2** and ratiometric analysis of the molecular rotor **1**

As is known, solvent viscosity influences the rate of the non-radiative deactivation process coming from intramolecular rotation in a fluorophore.<sup>15</sup> In that sense, Förster and Hoffmann described a relationship between solvent viscosity ( $\eta$ ) and fluorescence quantum yield ( $\Phi_F$ ).<sup>16</sup> Accordingly, the relationship should be described by eqn. (1):

$$\Phi_f = z\eta^\alpha \quad \text{eqn. (1)}$$

where  $z$  and  $\alpha$  are constants. Then a plot of  $\log \Phi_f$  vs.  $\log \eta$  should yield a straight line with slope  $\alpha$ .

As mentioned above, Figure 3 shows the fluorescence spectra of **1** and **2** in solvents of different viscosity but similar polarity properties. Interestingly, a new red-shifted band at 535 nm appears in **1** and no bathochromic effect is observed when changing the polarity from *i*-propanol (*i*-PrOH,  $\epsilon = 20.18$ ) to propylene glycol (PG,  $\epsilon = 32.0$ ), however, in the case of **2** a subtle bathochromic shifting of *ca.* 40 nm is observed. Moreover, the red-shifted band at 535 nm in **1** is only observed in the highly viscous solvents MET and PG, highlighting a selective turn-on fluorescence effect. These results also show the impact of electronic coupling through the  $\pi$ -molecular bridge present in the probes, causing a small ICT process in **2** but no charge transfer interactions in **1**. This observation was further confirmed by solvatochromic analyses and theoretical computations, see the next sections.

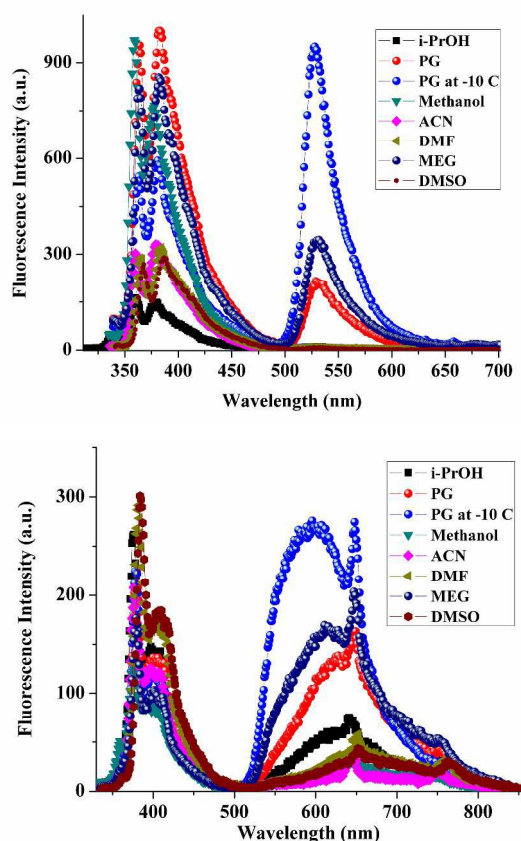
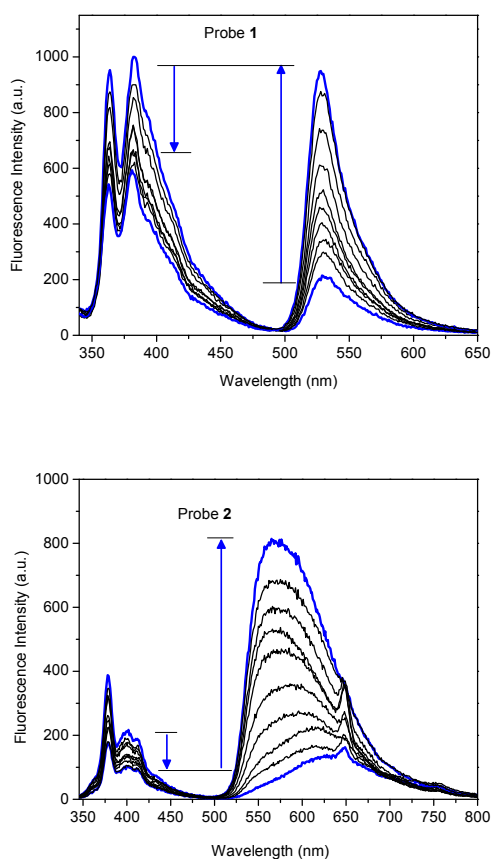


**Figure 3.** Fluorescence emission spectra of 1  $\mu$ M probes **1** (above,  $\lambda_{\text{ex}} = 385$  nm) and **2** (below,  $\lambda_{\text{ex}} = 345$  nm) in solvents of similar polarity but different viscosity values. *i*-

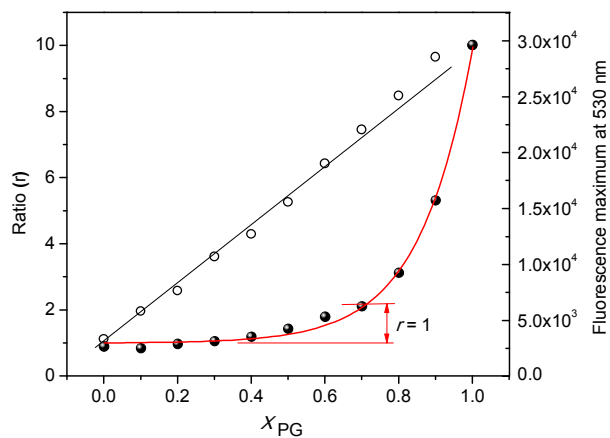
propanol (*i*-PrOH,  $\epsilon = 20.18$ ,  $\eta = 2.038$  cP); propylene glycol (PG,  $\epsilon = 35.1$ ,  $\eta = 45$  cP); methanol ( $\epsilon = 32.6$ ,  $\eta = 0.59$  cP); acetonitrile (ACN,  $\epsilon = 37.5$ ,  $\eta = 0.38$  cP); dimethylformamide (DMF,  $\epsilon = 36.7$ ,  $\eta = 0.82$  cP); monoethylene glycol (MEG,  $\epsilon = 37.7$ ,  $\eta = 20$  cP); dimethyl sulfoxide (DMSO,  $\epsilon = 46.6$ ,  $\eta = 2.0$  cP). Note: the sharp features in the long wavelength emission of **2** correspond to the spectrophotometer lamp noise.<sup>17</sup>

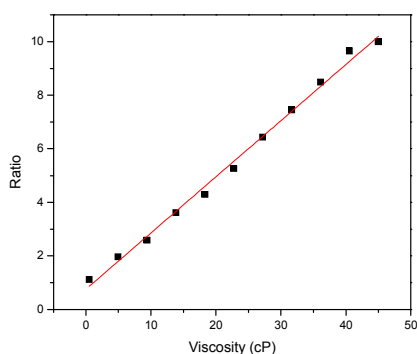
In addition, a  $\lambda$ -ratiometric response was confirmed for both probes. The ratiometric viscosity sensor incorporates two independent chromo-fluorophores, fluorene and 5-aryl-BODIPY. Here, fluorene is not influenced by viscosity changes and is used to control the concentration features like absorbance variations. On the other hand, 5-phenyl-BODIPY in **1** or 5-thiophen-BODIPY in **2**, act as molecular rotors with viscosity fluorescence sensitivity. Thus, the ratiometric fluorescence detection of these probes should allow viscosity to be measured without the bias associated with chromophore concentration. Figure 4 shows the fluorescence spectra obtained for **1–2** in a medium of increased molar fraction of PG. Small changes in the fluorene emission intensities can be seen, in particular for **2**.

Figure 5A shows the analytical range of propylene glycol molar fraction ( $X_{PG}$ ) from which probe **1** allows the quantitative analysis of microviscosity with a detection limit less than  $X_{PG}$  0.7 (at  $r = 1$ ) in a linear dynamic range from 0 to 9.8 (solid circles). On the other hand, the open circles show the ratiometric response defined as the ratio of fluorescence intensities at 530 and 380 nm ( $r_{530/380}$ ), demonstrating a remarkable improvement in the analytical method since the linear range extends now *ca.* 9 fold from 1.11 to 9.98 with a linear behavior up to 0.85 molar fraction of PG, representing a critical advantage.



**Figure 4.** Fluorescence spectra of 1  $\mu\text{M}$  **1** ( $\lambda_{\text{ex}} = 385 \text{ nm}$ ) and **2** ( $\lambda_{\text{ex}} = 345 \text{ nm}$ ) in a medium of increased molar fraction of PG:Methanol ranging from [10:90, 20:80, 30:70, 40:60, 50:50, 60:40, 70:30, 80:20, 90:10 and 100:0 v/v], respectively.





**Figure 5.** Ratiometric analysis using the ratio  $r$  of intensities at 530 and 380 nm ( $r_{530/380}$ ) vs. propylene glycol molar fraction ( $X_{PG}$ ) for **1**. The fluorescence intensity maximum at 530 nm is represented in solid circles while the ratio of intensities in open circles, (above). The fluorescence ratiometric calibration plot against microviscosity for **1** using eqn (1), (below).

For that reason, choosing a constant excitation wavelength, the ratiometric response of probe **1** can be calibrated against viscosity according to eqn. (1) through a low sensitive viscosity detection range from 0 to 45 cP, Figure 5B. However, the microviscosity range can be extended if required by using more viscous media. As mentioned in Figure 5B, the fluorescence ratiometric calibration vs. microviscosity plot for **1** using eqn (1), resulted in  $\alpha = 0.513$ . Again, it is important to mention that calibration for probe **2** is more susceptible to polarity interference, for this reason we only focus the ratiometric analysis for probe **1**.

## 2.5. Fluorescence anisotropy measurements for probes 1-2

Recently, steady state and time-resolved fluorescence anisotropy measurements have been widely used to measure local viscosity effects in the microenvironment of fluorophores. The Perrin equation describes the fluorescence anisotropy of a fluorophore according to eqn. (2):<sup>18</sup>

$$\frac{1}{r} = \frac{1}{r_0} \left( 1 + \frac{\tau_f}{\tau_c} \right) \quad \text{eqn. (2)}$$

where  $r$  is the measured anisotropy,  $r_0$  is the initial anisotropy and  $\tau$  is the rotational correlation time of the molecular probes.

Fluorescent molecular rotors, which typically have  $\alpha$  [from eqn. (1)] values in the range 0.3–0.75,<sup>19</sup> will have a markedly different anisotropy dependence on the viscosity compared to rigid molecules where  $\alpha = 0$ .

Figure 6 shows the obtained anisotropy measurements of **1–2** for a series of propylene glycol molar fractions, the plot is presented as a logarithmic viscosity scale in cP vs. anisotropy  $r$  in order to clearly visualize the dynamic range provided for **1–2**. In both cases, it can be observed that up to 5 cP a strong increase in anisotropy is obtained and this trend does not reach saturation, suggesting that a more viscous media is required. Both, **1–2** exhibit similar dynamic ranges being lower in the case of probe **2**, however.

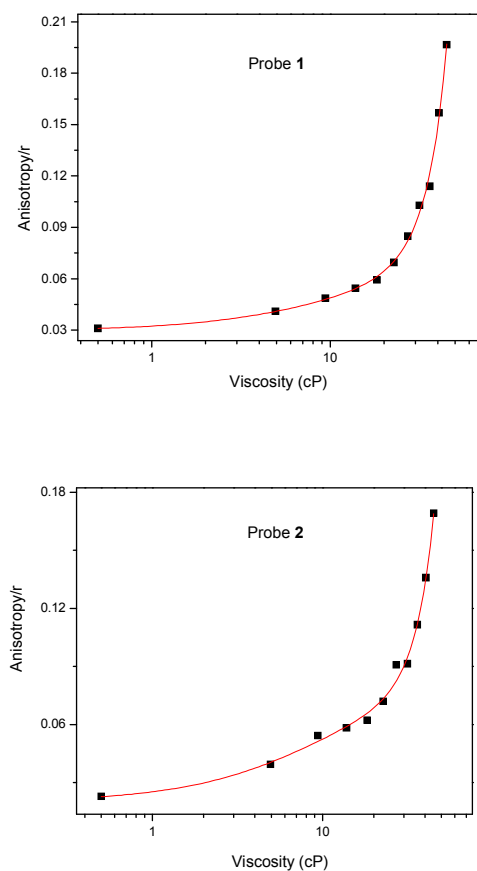


**Figure 6.** Viscosity variations of a propylene glycol:methanol mixtures vs. fluorescence steady state anisotropy ( $r$ , excitation at 505 nm and emission at 570 nm) for probes **1** and **2**. Here the PG:Methanol mixtures range from [0:100, 10:90, 20:80, 30:70, 40:60, 50:50, 60:40, 70:30, 80:20, 90:10 and 100:0 v/v], respectively.

## 2.6. Dipole moment changes upon photo-excitation and specific solvent effects

The effect of solvent interactions on the absorption and emission spectra of probes **1** and **2** was first investigated in terms of the Lippert–Mataga approximation. This description is based on the analysis of the linear relationship between the solvent polarity parameter (orientation polarizability) and the experimental Stokes shift obtained in a series of solvents. In particular, the Lippert theory considers that the absorption and emission spectral shifts are due to specific solvent effects; where hydrogen bonding and CT interactions exert a major influence; however, several specific interactions can also give nonlinear Lippert plots, such as preferential solvation, acid-base effects and hydrogen bonding (solvent-solute).<sup>20</sup> The Lippert-Mataga equation relates Stokes shift and solvent polarity according to eqn. (3):

$$\Delta \bar{\nu} = \bar{\nu}_A - \bar{\nu}_F = \frac{2}{hc} (\Delta f) \frac{(\mu_e - \mu_g)^2}{a^3} + C \quad \text{eqn. (3)}$$

where  $\bar{\nu}_A$  and  $\bar{\nu}_F$  are the wavenumbers (in  $\text{cm}^{-1}$ ) of the absorption and emission, respectively,  $h$  is Planck's constant,  $c$  is the speed of light,  $a$  is the Onsager radius, and  $\Delta\mu = \mu_e - \mu_g$  is the dipole moment difference between the ground and excited states. The orientation polarizability  $\Delta f$  is defined in terms of the dielectric constant ( $\epsilon$ ) and the refractive index ( $n$ ) of the solvent as (eqn. 4). When Lippert-Mataga plots exhibit a linear behavior, the general solvent effects are dominant in the spectral shifts.

$$\Delta f = f(\epsilon) - f(n^2) = \left( \frac{\epsilon - 1}{2\epsilon + 1} - \frac{n^2 - 1}{2n^2 + 1} \right) \quad \text{eqn. (4)}$$

When a non-linear behavior is observed, the specific solvent effects govern the spectral shifts offering an evidence of specific solute-solvent interactions. It can be seen in Figure 7 that the absorption band does not display significant shifts due to variations in solvent polarity. Similarly, no red-shifting is observed in the fluorescence spectra when the polarity increases, suggesting a small dipole moment change between the excited- and ground-states ( $\Delta\mu_{e-g}$ ). In order to have experimental evidence of the intramolecular charge transfer process taking place in **1** and **2**, the values can be calculated from Lippert-Mataga plots. As can be seen in Figure 8, the obtained Lippert plots resulted to have some non-linear behavior and  $\Delta\mu_{e-g}$  value cannot be properly obtained. Since no hydrogen-bond

interactions are expected to be relevant, and no ICT process was observed, more specific interactions need to be analyzed to account for such a Lippert behavior. In fact, the Lippert plot for **1–2** is almost flat, indicating little change in the dipole moment upon excitation and no determinable charge-transfer properties for these molecules, Figure 8.

As it was mentioned, the influence of solvent polarity exerts a dramatic impact on the microviscosity calibration of the probes. To give an example, for the well-known dual-fluorescent probe dimethylamino(benzonitrile), DMABN, it has been shown that the influence of polarity on emission intensity is so large that it could not be separated from the effect of viscosity.<sup>12</sup> In this vein, the above results indicate that although probe **2** is prone to have subtle solvent polarity interactions, in general it has almost no polarity interference, while probe **1** has no viscosity interference at all.

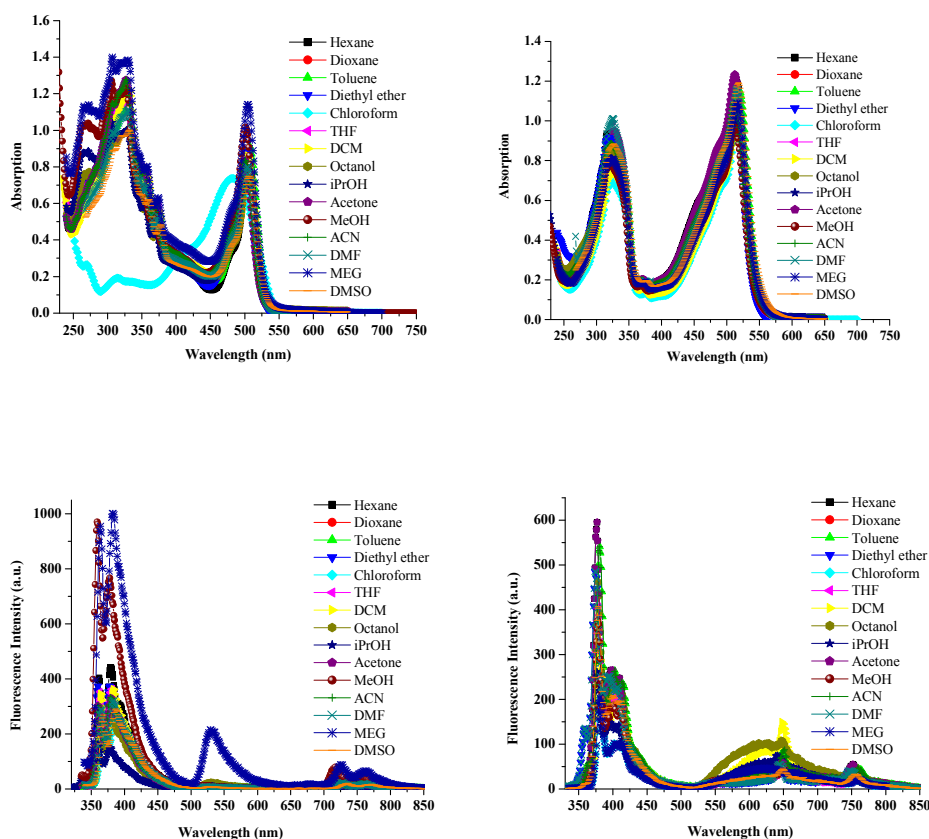




**Figure 7.** Absorption (above) spectra of 30  $\mu\text{M}$  **1** (left) and **2** (right) and fluorescence (below) of 1  $\mu\text{M}$  **1** (left,  $\lambda_{\text{ex}} = 385 \text{ nm}$ ) and **2** (right,  $\lambda_{\text{ex}} = 345 \text{ nm}$ ) obtained in different solvents.

**Table 2.** UV-Vis absorption and emission data for **1** (and **2**).<sup>a</sup>

Solvent	$\epsilon$	$n$	$Af$	$\lambda_a \text{ (nm)}$	$\bar{\nu}_a \text{ (cm}^{-1}\text{)}$	$\lambda_e \text{ (nm)}$	$\bar{\nu}_e \text{ (cm}^{-1}\text{)}$	$\bar{\nu}_a - \bar{\nu}_e$
Hexane	2.02	1.4235	0	313 (314)	31948 (31847)	360 (375)	27777 (26666)	4171 (5181)
Dioxane	2.22	1.4224	0.021	314 (315)	31847 (31746)	362 (376)	27624 (26595)	4223 (5151)
Toluene	2.38	1.4961	0.013	316 (319)	31645 (31348)	364 (380)	27472 (26315)	4173 (5033)
Diethyl ether	4.267	1.3526	0.165	315 (314)	31746 (31847)	360 (377)	27777 (26525)	3969 (5322)
Chloroform	4.81	1.4459	0.148	-----	-----	367 (381)	27248 (26246)	-----
THF	7.52	1.4050	0.210	314 (315)	31847 (31746)	363 (381)	27548 (26246)	4299 (5500)
DCM	8.93	1.4242	0.217	314 (316)	31847 (31645)	364 (382)	27472 (26178)	4375 (5467)
Octanol	10.30	1.4295	0.225	316 (317)	31645 (31545)	365 (382)	27397 (26178)	4248 (5367)
<i>i</i> -PrOH	20.18	1.3776	0.277	315 (315)	31746 (31746)	365 (380)	27397 (26315)	4349 (5431)
Acetone	21.01	1.3588	0.285	313 (314)	31949 (31847)	364 (380)	27472 (26315)	4477 (5532)
MeOH	33.00	1.3288	0.308	316 (313)	31645 (31948)	363 (381)	27548 (26246)	5399 (5702)
ACN	36.64	1.3442	0.305	316 (315)	31645 (31746)	364 (384)	27472 (26041)	4173 (5705)
DMF	36.70	1.4305	0.274	315 (316)	31746 (31645)	365 (380)	27397 (26315)	4349 (5330)
MEG	41.40	1.4320	0.276	316 (317)	31645 (31545)	366 (384)	27322 (26041)	4323 (5504)
DMSO	46.68	1.4793	0.263	317 (318)	31545 (31446)	368 (381)	27174 (26246)	4371 (5200)
PG	32.00	1.432	0.138	320 (322)	31250 (31055)	371 (380)	26954 (26315)	4296 (4740)

<sup>a</sup> Dielectric constant, ( $\epsilon$ ), refractive index, ( $n$ ); <sup>2f</sup> Orientation polarizability, ( $Af$ ); absorption wavelength, ( $\lambda_a$ ); absorption wavenumber, ( $\bar{\nu}_a$ ); emission wavelength, ( $\lambda_e$ ); emission wavenumber, ( $\bar{\nu}_e$ ) for compounds **1** (and **2** in parenthesis). Solvent notation: THF (tetrahydrofuran), DCM (dichloromethane), *i*-PrOH (*iso*-propanol), MeOH (methanol), ACN (acetonitrile), DMF (dimethylformamide), MEG (ethylene glycol), DMSO (dimethyl sulfoxide), PG (propylene glycol).

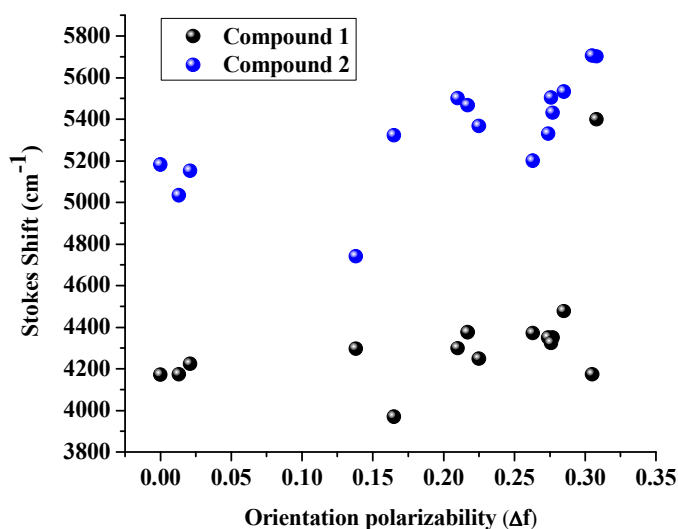


**Figure 8.** Lippert plots for compounds **1** and **2**.

It is important to mention that a more systematic solvatochromic analysis is required in order to establish additional specific solvent interactions which can interfere with the microviscosity calibration. This is done by the use of empirical solvatochromic scales. More recently, an empirical methodology to explain experimental solvatochromic properties of chromophores from theoretical solvent characteristics was developed by Catalán.<sup>22</sup> This systematic analysis is only possible with Catalán solvent scale since it offers a solvent polarity/polarizability parameters separation. It is well known that the relationship between solvent effects and spectral shifts can be denoted by a multilinear equation.<sup>23</sup> The mathematical treatment of solvent effects introduced by Catalán is based on four empirical and independent solvent scales.

$$y = y_0 + a_{SA} SA + b_{SB} SB + c_{SP} SP + d_{SdP} SdP \quad \text{eqn. (5)}$$

Here SA, SB, SP and SdP are the solvent acidity, basicity, polarizability and dipolarity properties, respectively. The coefficients  $a_{SA}$ ,  $b_{SB}$ ,  $c_{SP}$  and  $d_{SdP}$  represent the contribution of each type of interactions. Thus, a Catalán solvent analysis was carried out in order to understand the solvent parameters that affect the photophysical properties ( $\bar{\nu}_{\text{abs}}$ ,  $\bar{\nu}_{\text{em}}$  and  $\Delta\bar{\nu}$ ) in probes **1-2**. The {SA, SB, SP, SdP} parameters for each solvent are taken from reference (22).

The regression coefficients  $y_0$ ,  $a_{SA}$ ,  $b_{SB}$ ,  $c_{SP}$  and  $d_{SdP}$ , standard errors and the multilinear correlation coefficient,  $r$ , for **1–2** are presented in Table 3. In the case of **1**, we obtained a good multilinear fit of 0.914 only for the  $\bar{\nu}_{em}$  observable. Interestingly, the analysis indicates that the major factor contributing to the solvatochromic changes in  $\bar{\nu}_{em}$  is the solvent polarizability (separated from polarity), since the coefficient value  $c_{SP}$  is larger and has the smallest standard error. Moreover, the SdP parameter does not affect the fluorescence response importantly in **1** because the multilinear regression without considering SP gives a slightly lower  $r$ -value according to eqn. (5), namely, 0.874 for {SP,SA,SB} variables, corroborating that **1** displays no important sensitivity to solvent polarity. That behavior results interesting and has been described for some dual-fluorescence probes.<sup>24</sup> This is in agreement with the push-pull character of the molecule, observing a poor linear correlation of 0.78 between the dielectric constant ( $\epsilon$ ) and  $\bar{\nu}_{em}$ , because specific effects are also taking place. In the case of **2**, we observed the same result having good multilinear fits of 0.882, 0.845 and 0.917 for  $\bar{\nu}_{abs}$ ,  $\bar{\nu}_{em}$ , and  $\Delta\bar{\nu}$ , respectively. Again, the polarizability of the medium is dominant in the spectroscopic properties studied, although solvent polarity exerts a small influence. This behavior is difficult to achieve in common fluorophores due to the strong dependence on the molecular electron redistribution upon photoexcitation. Moreover,  $\bar{\nu}_{abs}$  reaches poor multilinear regression coefficients suggesting that solvent viscosity parameter may influence the solvatochromic analysis.

**Table 3.** Estimated coefficients  $y_0$ ,  $a_{SA}$ ,  $b_{SB}$ ,  $c_{SP}$  and  $d_{SdP}$  for  $\bar{\nu}_{abs}$ ,  $\bar{\nu}_{em}$ , and  $\Delta\bar{\nu}$  ( $\text{cm}^{-1}$ ) and multiple correlation coefficient ( $r$ ) for regression analysis of compound **1** (**2** in Table S1†) in 16 solvents according to the Catalán solvent parameters {SA, SB, SP, SdP}.

Observable	$y_0$ ( $\text{cm}^{-1}$ )	$a_{SA}$	$b_{SB}$	$c_{SP}$	$d_{SdP}$	$r$
$\bar{\nu}_{abs}$	$32278 \pm 314$	$-193 \pm 149$	$-82 \pm 143$	$-612 \pm 447$	$-48 \pm 113$	0.701
$\bar{\nu}_{em}$	$28608 \pm 215$	$-75 \pm 102$	$-125 \pm 97$	$-1256 \pm 305$	$-246 \pm 77$	0.914
$\Delta\bar{\nu}$	$4900 \pm 776$	$670 \pm 369$	$-224 \pm 353$	$-1128 \pm 1104$	$379 \pm 280$	0.742

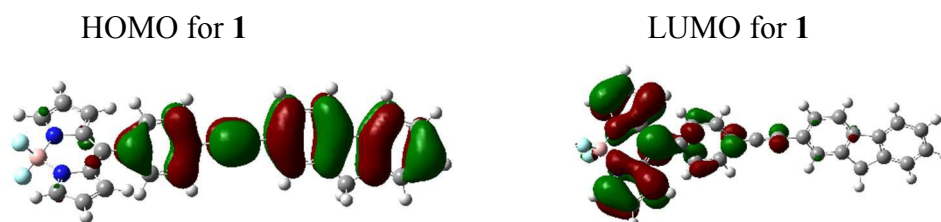
Finally, it is worth mentioning that the estimated  $c_{SP}$  values significantly differ (within experimental error) for absorption and emission, this is expected when no van der Waals type interactions with the solvent are taking place. Then, the electronic structure of

the Franck-Condon and relaxed excited states is quite different. This observation is highly relevant since for a molecule with poor acid-base solvent interactions, the Franck-Condon and relaxed excited states can only be different due to the strong rotational motion present in the BODIPY -derived fluorescent molecular rotor.

## 2.7. DFT and TD-DFT calculations of photophysical properties for 1-2

As it was mentioned, probes **1-2** have no ICT character since the phenyl-acetylene  $\pi$ -bridge is not so efficient to promote charge redistribution upon photoexcitation. However, careful inspection on the HOMO-LUMO localization suggests that in these geometries an ICT character should not be ignored. In fact, the HOMO level is more located toward the fluorene fragment and LUMO level is localized in the BODIPY fragment.

DFT calculations at a B3LYP/6-31+G(d,p)/PCM (Methanol) level of theory were used to determine the optimized molecular geometry for **1-2**. Then, a frequency analysis corroborates that these geometries correspond to an energy minimum. As a first step in the analysis of the electron charge distribution in the molecules, the electrostatic potentials for **1** and **2** were computed, observing no important differences in the local charge distribution between the molecules, i.e. most of the molecular surface is neutral in charge, Figure 9. However, frontier molecular orbitals (FMOs) reveal a D- $\pi$ -A dipolar nature in the molecules. The isodensity plots of the HOMO-LUMO orbitals at the same level of theory are also shown in Figure 9. Then, a deeper understanding in the calculated ICT properties is mandatory. Obviously, no ICT character was observed experimentally, and the role of the  $\pi$ -bridge was paramount.



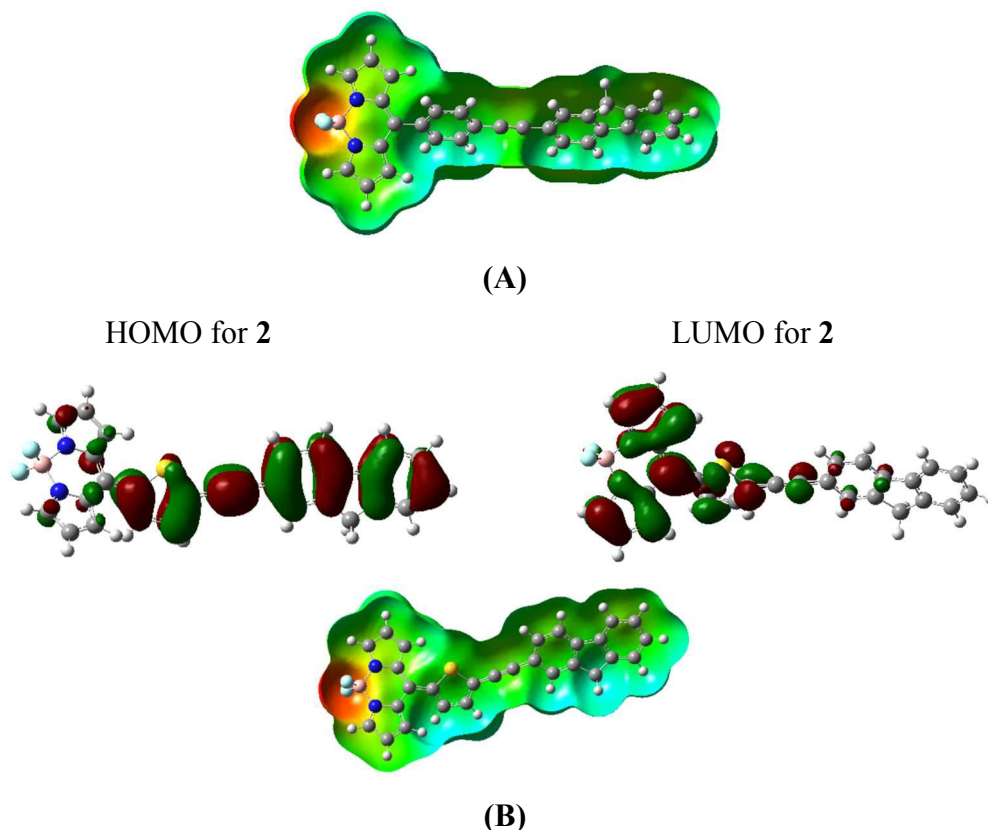


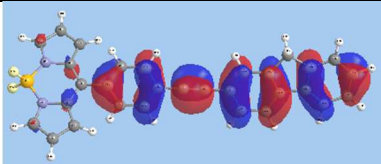
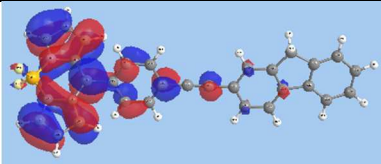
**Figure 9.** Computed (PBE0/6-31G(d)/PCM) HOMO-LUMO orbitals together with electrostatic potential mapped onto total electron density for the ground state for **1** (A) and **2** (B). Areas marked in red gain electric charge, while cyan and blue are depleted of electron density in the ground state. Green color depicts neutral regions.

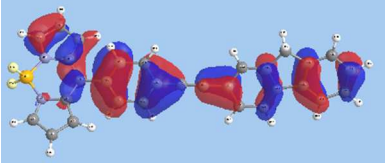
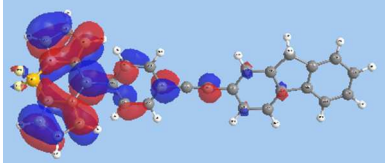
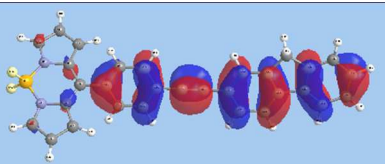
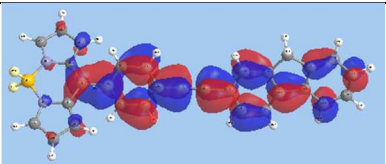
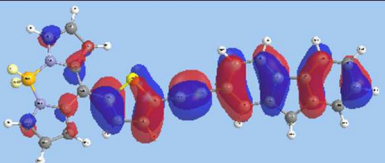
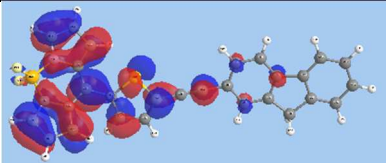
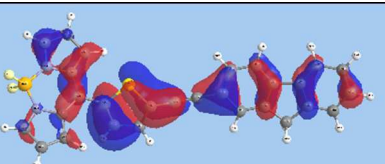
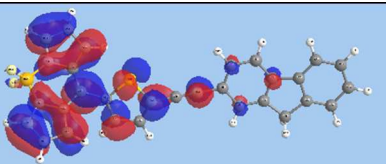
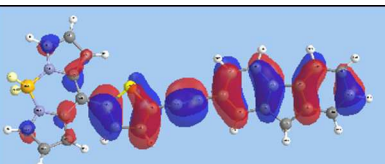
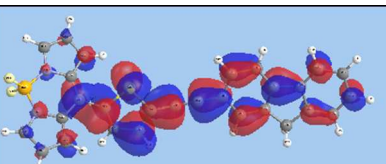
First, we employed TD-DFT to elucidate the optical properties of **1–2**. The obtained UV-Vis absorption spectrum by means of oscillator strength parameters supports the spectral pattern experimentally observed. Indeed, a three band pattern corresponding to the  $S_{0-0}$  and  $S_{0-1}$  bands of the fluorene fragment and the BODIPY -derived band. Also, the red-shifting in the corresponding spectrum for compound **2** is reproduced, Figure S9†.

TD-DFT provides a good benchmark in the determination of spectroscopic properties due to the accurate description of ground and excited potential energy surfaces. However, in most of the cases, conventional TD-DFT results in a description of an excited state in terms of several single electronic excitations from an occupied to a virtual orbital. Fortunately, the various contributions to the electronic excitation can be clarified by a Natural Transition Orbital (NTO) analysis,<sup>25</sup> which provides a compact orbital

representation of the electronic transition through a single configuration of a *hole* and *electron* interaction in a given state. Consequently, the photoinduced electron transfer process is not depicted by a simple change in the elementary molecular orbital occupancy, but in a hole-electron distribution.

Figure 10 shows the NTO distribution for **1-2**. It is to be noted that both molecules can be viewed as planar dipolar structures, having  $C_2$  symmetry. Therefore, the electronic transition from the ground ( $|g\rangle$ ) to the first excited ( $|e_1\rangle$ ) state can be represented as  $1A \rightarrow 2A$ . Thus, for probe **1** the hole is spread along the phenyl-ethynyl-fluorene axis, while the electron is mainly spread in the BODIPY unit with a contribution of the phenyl-ethynyl bridge, which confers a small dipolar polarization, giving in fact a slight ICT character to the  $1A \rightarrow 2A$  transition. The parameters for this electronic transition are shown in Figure 10, providing the wavelength value in nanometers, the oscillator strength and the NTO coefficient ( $w$ ) representing the extent to which the electronic excitation can be written as a single excitation. Moreover, the low-energy band experimentally observed near 500 nm can be ascribed to the HOMO-LUMO levels by simple comparison with the calculated spectrum of **1**. A similar pattern is observed for the HOMO-1-LUMO configurations, but in the case of the HOMO-LUMO+1 configurations both, the hole and electron are localized in the phenyl-ethynyl-fluorene fragment (not in BODIPY) giving rise to the more energetic absorption band experimentally observed around 320 nm. Importantly, this electron redistribution highlights the potential of the probe as microviscosity probes since both, the ethynyl-fluorene and the phenyl-BODIPY fragments can respond to local-viscosity changes.<sup>26</sup> On the other hand, for probe **2** we observed a similar behavior although more charge transfer character is present, making it more susceptible to solvent polarity changes.

Absorption	Hole (probe <b>1</b> )	Electron (probe <b>1</b> )
530.6 nm $f = 0.532$ $w = 0.70$ HOMO-LUMO		

433.1 nm $f = 0.445$ $w = 0.69$ HOMO-1-LUMO		
349.5 nm $f = 0.445$ $w = 0.69$ HOMO-LUMO+1		
Absorption	Hole (probe 2)	Electron (probe 2)
573.0 nm $f = 0.775$ $w = 0.70$ HOMO-LUMO		
449.5 nm $f = 0.393$ $w = 0.69$ HOMO-1-LUMO		
362.3 nm $f = 1.016$ $w = 0.67$ HOMO-LUMO+1		

**Figure 10.** Natural Transition Orbitals (NTOs) computed at PBE0/6-31+G(d,p)/PCM-Methanol for **1** and **2**. The left column shows the wavelength value in nanometers, the oscillator strength ( $f$ ), the NTO eigenvalue ( $w$ ) and the MO occupation.

Finally, in order to better analyze the degree of dipolar polarization observed in the NTO hole-electron interactions particularly for the HOMO-LUMO configurations, we studied the charge transfer excitation by means of the recently proposed spatial extent index<sup>27</sup> at a PBE0/G-31+G(d,p)/PCM (Methanol) level of theory. For probe **1**, the obtained fraction of electron charge transferred upon excitation was  $q_{CT} = 0.53$  at a  $D_{CT} = 7.18$  Å spatial distance from the donor centroid to the acceptor centroid. The  $H$  index defined as half of the sum of the centroid axis along the Donor-Acceptor direction is 1.57, this leads to a slight overlap between donor and acceptor centroids, giving rise to an inefficient ICT



process. In the case of compound **2**, the amount of charge transferred was  $q_{CT} = 0.55$  at a  $D_{CT} = 7.95$  Å spatial distance. The  $H$  index for **2** was 1.22, this result also implies an inefficient ICT process in **2**.

### 3. Conclusion

Two novel fluorescent rotors as molecular microviscosity probes (**1–2**) were synthesized and characterized. This contribution is focused on the factors determining the ability of these probes to give a ratiometric respond to microviscosity. Through an integrated experimental and computational approach, the results demonstrate that **1** is a very sensitive probe to subtle changes in microviscosity, displaying no solvent polarity influence, which allows to calibrate the ratiometric response of the probe.

Particularly, it can be concluded that the probes do not display noticeable solvatochromic effects. However, careful evaluation of the solvent interactions revealed that the solvent polarizability parameter exerts an important influence on fluorescence properties, which is in agreement with the specific solvent microviscosity susceptibility.

The conjugation length-elongation strategy was used by introducing a triple bond linkage between fluorene and 5-aryl-BODIPY moieties, which was shown to be highly efficient in inhibiting the ICT process. This  $\pi$ -bridge is of capital importance, enhancing the viscosity sensitivity and precluding efficient ICT character as confirmed by the spatial extent of the charge transfer excitation index.

Finally, the fluorescent ratiometric response results are highly promising for the fast and reliable quantitative detection of microviscosity changes in the media, since simple changes in fluorescence intensity are of low analytical importance due to the absence of internal reference. In the case of the more promising probe **1**, a detection limit less than  $X_{PG}$  0.7 (at  $r = 1$ ) in a linear dynamic range from 0 to 9.8 was determined whose ratiometric response remarkably improves the analytical method since the linear range extends now *ca.* 9 fold with a linear behavior up to 0.85 molar fraction of PG.

### 4. Experimental section

#### 4.1 Chemicals



THF was dried over sodium and benzophenone, the *i*Pr<sub>2</sub>NH and CH<sub>2</sub>Cl<sub>2</sub> were dried over calcium hydride prior to use, pyrrole was distilled before use. 4-Bromobenzaldehyde, 5-bromo-2-thiophenecarboxaldehyde, CF<sub>3</sub>COOH, BF<sub>3</sub>·OEt<sub>2</sub>, triethylamine (Et<sub>3</sub>N), 2,3-dichloro-5,6-dicyano-1,4-benzoquinone (DDQ), bis(triphenylphosphine)palladium(II) dichloride (Pd(PPh<sub>3</sub>)<sub>2</sub>Cl<sub>2</sub>) and CuI, were purchased from Aldrich company and used without further purification. Column chromatography was performed on silica (60-120 mesh).

#### 4.2 Instrumentation

Infrared spectra were measured on a Perkin-Elmer Spectrum 400 FT-IR/FT-FIR spectrophotometer, wavenumber is reported in cm<sup>-1</sup>. <sup>1</sup>H NMR spectrum (δ in ppm) were recorded using Varian Unity Inova Autosuitable, 400 MHz spectrometer, <sup>13</sup>C NMR spectrum were recorded on Varian operating at 100.518 MHz. All experiments were made with concentrations between 30 and 40 mg/mL at 25 °C. Chemical shifts (ppm) are relative to Si(CH<sub>3</sub>)<sub>4</sub> for <sup>1</sup>H (of residual proton; δ 7.25 ppm) and <sup>13</sup>C (δ 77.0 ppm signal) in CDCl<sub>3</sub>. High-resolution mass spectra were obtained from Thermo-Electron DFS spectrometer instrument by the electron impact (EI) ionization technique. Absorption and fluorescence spectra were obtained with Perkin Elmer Lambda 2S UV/Vis spectrophotometer and Varian Cary Eclipse fluorescence spectrometer, respectively. Fluorescence spectra were recorded at 25 °C in a 1 cm quartz fluorescence cuvette placed in a thermostated holder at 25 ± 0.1 °C with a recirculating water bath. All fluorescence quantum yield measurements were obtained by using the experimental procedure reported in reference.<sup>28</sup>

#### 4.3 Computational method

Quantum Chemical Calculations were obtained by using DFT and TD-DFT with Polarizable Continuum Model<sup>29</sup> as performed in the Gaussian 09 code.<sup>30</sup>

#### 4.4. Syntheses

4.4.1. *meso*-(4-(9H-Fluoren-2-yl)ethynyl)phenyl-4,4-difluoro-4-bora-3a,4a-diaza-s-indacene (**1**)

In a 100 mL flask, compound **3** (200 mg, 0.60 mmol) was dissolved in 20 mL of anhydrous THF, after that, Pd(PPh<sub>3</sub>)<sub>2</sub>Cl<sub>2</sub> (21 mg, 0.03 mmol), 2-ethynyl-9H-fluorene **7** (171 mg, 0.09 mmol) and CuI (6 mg, 0.03 mmol) was added under constant bubbling of N<sub>2</sub>, finally *i*Pr<sub>2</sub>NH (0.2 mL, 1.2 mmol) was added dropwise. The crude reaction was supported on celite and purified by flash chromatography using hexane/ethyl acetate (90/10, v/v), thereby obtaining compound **1** as an orange solid in 70% yield (192 mg). mp 147-148 °C. <sup>1</sup>H NMR (500 MHz, CDCl<sub>3</sub>, δ in ppm): 3.95 (s, 2H, H-9'), 6.58 (dd, *J* = 1.4, 4.1 Hz, 2H, H-2), 6.97 (d, *J* = 4.1 Hz, 2H, H-1), 7.35 (td, *J* = 1.1, 7.4 Hz, 1H, H-7'), 7.41 (td, *J* = 1.1, 7.4 Hz, 1H, H-6'), 7.58 (dt, *J* = 1.9, 8.5 Hz, 2H, H-8), 7.57-7.59 (m, 2H, H-3', H-8'), 7.70 (dt, *J* = 1.9, 8.5 Hz, 2H, H-9), 7.77 (s, 1H, H-1'), 7.80 (d, *J* = 7.7 Hz, 1H, H-4'), 7.82 (d, *J* = 6.8 Hz, 1H, H-5'), 7.96 (s, 2H, H-3). <sup>13</sup>C NMR (125 MHz, CDCl<sub>3</sub>, δ in ppm): 36.9 (C-9'), 88.5 (C-11), 93.4 (C-12), 118.8 (C-2), 120.1 (C-4'), 120.5 (C-5'), 120.7 (C-2'), 125.3 (C-8'), 126.6 (C-10), 127.2 (C-6'), 127.5 (C-7'), 128.5 (C-1'), 130.8 (C-8), 130.9 (C-3'), 131.6 (C-1), 131.7 (C-9), 133.4 (C-6), 134.9 (C-5), 141.1 (C-10'), 142.6 (C-11'), 143.5 (C-13'), 143.8 (C-12') 144.4 (C-3), 146.7 (C-7). <sup>11</sup>B NMR (160 MHz, CDCl<sub>3</sub>, δ in ppm): -0.26 (t, *J*<sub>B-F</sub> = 28.7 Hz), <sup>19</sup>F NMR (470 MHz, CDCl<sub>3</sub>, δ in ppm): -411.24 (q, *J*<sub>B-F</sub> = 29.0 Hz). FT-IR (ATR, cm<sup>-1</sup>): 3112, 3066, 2958, 2925, 2857, 2201, 1558, 1385, 1258, 1099, 1075, 1044, 772, 734. HR-MS mass calcd. for C<sub>30</sub>H<sub>19</sub>BF<sub>2</sub>N<sub>2</sub> 456.1609; found *m/z* 456.1621.

#### 4.4.2. *meso*-(5-(9H-Fluoren-2-yl)ethynyl)thiophen-2-yl-4,4-difluoro-4-bora-3a,4a-diaza-*s*-indacene (**2**)

To obtain compound **2**, the procedure above described was followed; compound **4** (350 mg, 1.0 mmol), Pd(PPh<sub>3</sub>)<sub>2</sub>Cl<sub>2</sub> (35 mg, 0.05 mmol), the cocatalyst CuI (9 mg, 0.05 mmol), ethynylfluorene (283 mg, 1.5 mmol) were suspended in a round bottom flask and *i*Pr<sub>2</sub>NH (0.3 mL, 2.0 mmol) was added dropwise. The crude reaction was supported on celite and purified by flash chromatography column using hexane/ethyl acetate (90/10, v/v), thus obtaining compound **2** as a green solid in 61% yield (280 mg). mp 166-167 °C. <sup>1</sup>H NMR (400 MHz, CDCl<sub>3</sub>, δ in ppm): 3.93 (s, 2H, H-9'), 6.59 (d, *J* = 2.9 Hz, 2H, H-2), 7.31 (d, *J* = 4.1 Hz, 2H, H-1), 7.35 (t, *J* = 7.3 Hz, 1H, H-7'), 7.39-7.43 (m, 1H, H-6'), 7.40 (d, *J* = 3.9 Hz, 1H, H-9), 7.49 (d, *J* = 3.9 Hz, 1H, H-8), 7.57 (d, *J* = 4.3 Hz, 1H- H-3'), 7.58 (d, *J* = 4.1 Hz, 1H, H-8'), 7.73 (s, 1H, H-1'), 7.79 (d, *J* = 5.2 Hz, 1H, H-4'), 7.81 (d, *J* = 4.7 Hz,

1H, H-5'), 7.94 (s, 2H, H-3). <sup>13</sup>C NMR (125 MHz, CDCl<sub>3</sub>, δ in ppm): 36.9 (C-9'), 81.8 (C-12), 98.6 (C-11), 118.8 (C-2), 120.1 (C-2'), 120.1 (C-4'), 120.5 (C-5'), 125.3 (C-8'), 127.2 (C-6'), 127.7 (C-7'), 128.3 (C-1'), 130.3 (C-10), 130.7 (C-3'), 131.4 (C-1), 132.6 (C-9), 133.2 (C-8), 134.3 (C-6), 135.4 (C-5), 138.6 (C-7), 141.0 (C-10'), 143.0 (C-11'), 143.5 (C-13'), 143.8 (C-12'), 144.1 (C-3). <sup>11</sup>B NMR (160 MHz, CDCl<sub>3</sub>, δ in ppm): -0.32 (t, *J*<sub>B-F</sub> = 28.5 Hz), <sup>19</sup>F NMR (470 MHz, CDCl<sub>3</sub>, δ in ppm): -411.43 (dd, *J*<sub>B-F</sub> = 57.2, 28.6 Hz). FT-IR (ATR, cm<sup>-1</sup>): 3113, 3060, 2923, 2853, 2197, 1538, 1539, 1410, 1387, 1078, 768, 730. HR-MS mass calcd. for C<sub>28</sub>H<sub>17</sub>BF<sub>2</sub>N<sub>2</sub>S 462.1174; found *m/z* 462.1188.

#### 4.4.3. *meso*-(4-Bromophenyl)-4,4-difluoro-4-bora-3a,4a-diaza-*s*-indacene (3)

In a 250 mL round bottom flask *meso*-(4-bromophenyl)dipyrromethane **5** (1.2 g, 4.0 mmol) and DDQ (1.0 g, 4.41 mmol) were dissolved in 40 mL of anhydrous CH<sub>2</sub>Cl<sub>2</sub> and bubbled with N<sub>2</sub> for 10 min, after stirring the reaction for 30 min we added Et<sub>3</sub>N (1.2 mL, 8.98 mmol) and after 10 minutes, BF<sub>3</sub>·OEt<sub>2</sub> was added with a syringe and the reaction was stirred overnight, the progress of the reaction was monitored by thin-layer chromatography. Once consumed the starting dipyrromethane, the mixture was diluted with dichloromethane and washed with water and the organic phase was filtered over Na<sub>2</sub>SO<sub>4</sub>, the solvent was evaporated and the crude reaction was supported over celite, the compound was purified by flash chromatography with hexane/ethyl acetate (85/15, v/v) as eluent. The *meso*-(4-bromophenyl)-4,4-difluoro-4-bora-3a,4a-diaza-*s*-indacene **3** was obtained as a green solid in 67% (0.92 g) yield. mp 198-200 °C. <sup>1</sup>H NMR (400 MHz, CDCl<sub>3</sub>, δ in ppm): 6.56 (d, *J* = 4.1 Hz, 2H, H-2), 6.91 (d, *J* = 4.2 Hz, 2H, H-1), 7.45 (dt, *J* = 2.4 and 8.5 Hz, 2H, H-8), 7.69 (dt, *J* = 2.4 and 8.5 Hz, 2H, H-9), 7.96 (s, 2H, H-3). <sup>13</sup>C NMR (100.5 MHz, CDCl<sub>3</sub>, δ in ppm): 118.8 (C-2), 125.5 (C-10), 131.3 (C-1), 131.8 (C-8 and C-9), 132.6 (C-6), 134.7 (C-5), 144.6 (C-3), 145.8 (C-7). <sup>11</sup>B NMR (128.3 MHz, CDCl<sub>3</sub>, δ in ppm): -0.35 (t, *J* = 28.5 Hz). <sup>19</sup>F NMR (282.4 MHz, CDCl<sub>3</sub>, δ in ppm): -144.93 (dd, *J* = 57.0, 28.5 Hz). FT-IR (ATR, cm<sup>-1</sup>): 3136, 3109, 1568, 1541, 1383, 1259, 1115, 1071, 774, 740. HR-MS mass calcd. for C<sub>15</sub>H<sub>10</sub>BBF<sub>2</sub>N<sub>2</sub> 346.0088; found *m/z* 346.0050.

#### 4.4.4. *meso*-(5-Bromothiophen-2-yl)-4,4-difluoro-4-bora-3a,4a-diaza-*s*-indacene (4)

Compound **6** (1.1 g, 3.13 mmol) and DDQ (0.78 g, 3.44 mmol) were dissolved in 40 mL of CH<sub>2</sub>Cl<sub>2</sub> with Et<sub>3</sub>N (0.90 mL, 6.47 mmol) and BF<sub>3</sub>·Et<sub>2</sub>O, under conditions similar to those used to obtain **3**. The compound *meso*-(5-bromothiophen-2-yl)-4,4-difluoro-4-bora-3a,4a-diaza-*s*-indacene **4** was obtained as a green solid, 63% (79 g) yield. mp 112-114 °C. <sup>1</sup>H NMR (400 MHz, CDCl<sub>3</sub>, δ in ppm): 6.59 (d, *J* = 2.8 Hz, 2H, H-2), 7.24 (d, *J* = 4.0 Hz, 2H, H-1), 7.25 (d, *J* = 4.2 Hz, H-8), 7.32 (d, *J* = 3.9, 1H, H-9), 7.93 (s, 2H, H-3). <sup>13</sup>C NMR (100.5 MHz, CDCl<sub>3</sub>, δ in ppm): 118.8 (C-2), 119.1 (C-10), 131.2 (C-1 and C-8), 133.1 (C-9), 134.0 (C-6), 135.8 (C-5), 137.9 (C-7), 144.3 (C-3). <sup>11</sup>B NMR (128.3 MHz, CDCl<sub>3</sub>, δ in ppm): -0.28 (t, *J*<sub>B-F</sub> = 28.7 Hz). <sup>19</sup>F NMR (282.4 MHz, CDCl<sub>3</sub>, δ in ppm): -145.99 (dd, *J*<sub>B-F</sub> = 57.4, 28.6 Hz). FT-IR (ATR, cm<sup>-1</sup>): 3106, 1542, 1410, 1385, 1263, 1117, 1076, 964, 756, 730. HR-MS mass calcd. for C<sub>13</sub>H<sub>8</sub>BBrN<sub>2</sub>S 351.9653; found *m/z* 351.9630.

#### 4.4.5. *meso*-(4-Bromophenyl)dipyrromethane (**5**)

In a 250 mL round bottom flask, *p*-bromobenzaldehyde (2g, 10.87 mmol) and pyrrole (6 mL, 86.96 mmol), were mixed together and the resulting mixture was bubbled with N<sub>2</sub> for 10 min, then trifluoroacetic acid (125 μL 1.62 mmol) was added. The solution was stirred at room temperature for 30 min, the progress of the reaction was monitored by TLC, when the disappearance of the starting aldehyde was observed, CH<sub>2</sub>Cl<sub>2</sub> and 0.1 M NaOH was added to the mixture and the organic phase was washed with water and filtered over Na<sub>2</sub>SO<sub>4</sub>, then solvent was evaporated and the crude product was supported on celite, the compound was purified by flash chromatography using an hexane/ethyl acetate/Et<sub>3</sub>N (85/15/1, v/v/v) mixture as eluent, thus obtaining the *meso*-(4-bromophenyl)dipyrromethane **5** as a white solid 85% (2.78 g) yield. <sup>1</sup>H NMR (400 MHz, CDCl<sub>3</sub>, δ in ppm): 5.42 (s, 2H, H-6), 5.88 (dd, *J* = 1.2 and 3.2 Hz, 2H, H-3), 6.15 (dd, *J* = 3.1 and 6.0 Hz, 2H, H-2), 6.70 (ddd, *J* = 1.5, 2.7 and 4.2 Hz, 2H, H-1), 7.08 (dt, *J* = 1.8 and 9.0 Hz, 2H, H-8), 7.43 (dt, *J* = 1.8 and 9.1 Hz, 2H, H-9), 7.89 (s, 2H, H-5). <sup>13</sup>C NMR (100.5 MHz, CDCl<sub>3</sub>, δ in ppm): 43.4 (C-6), 107.4 (C-3), 108.6 (C-2), 117.5 (C-1), 120.8 (C-10), 130.1 (C-8), 131.7 (C-9), 131.8 (C-4), 141.2 (C-7). FT-IR (ATR, cm<sup>-1</sup>): 3332, 3131, 3092, 1553, 1490, 1404, 1259, 1075, 762, 725. HR-MS mass calcd. for C<sub>15</sub>H<sub>13</sub>BrN<sub>2</sub> 300.0262; found *m/z* 300.0278.

#### 4.4.6. *meso*-(5-Bromothiophen-2-yl)dipyrromethane (**6**)

Compound **6** was obtained under the conditions established to obtain compound **5**, using 5-bromo-2-thiophencarboxaldehyde (2 g, 10.47 mmol) with pyrrole (5.8 mL, 83.75 mmol) and trifluoroacetic acid (242  $\mu$ L, 35.81 mmol) as starting materials, the compound was purified by flash chromatography using an hexane/ethyl acetate/Et<sub>3</sub>N (75/25/1, v/v/v) mixture as eluent. The *meso*-(5-bromothiophen-2-yl)dipyrromethane **6** was obtained as a white solid 84% (2.8 g) yield. <sup>1</sup>H NMR (400 MHz, CDCl<sub>3</sub>,  $\delta$  in ppm): 5.65 (s, 1H, H-6), 6.06 (ddd,  $J$  = 0.8, 1.6 and 3.6 Hz, 2H, H-3), 6.17 (dd,  $J$  = 2.8 and 6 Hz, 2H, H-2), 6.64, (dd,  $J$  = 0.8 and 3.6 Hz, 1H, H-8), 6.72 (ddd,  $J$  = 1.6, 2.8 and 4.4 Hz, 2H, H-1), 6.89 (d,  $J$  = 3.6 Hz, 1H, H-9), 7.80 (s, 2H, H-5). <sup>13</sup>C NMR (100.5 MHz, CDCl<sub>3</sub>,  $\delta$  in ppm): 39.4 (C-6), 107.3 (C-3), 108.6 (C-2), 111.1 (C-10), 117.7 (C-1), 125.8 (C-8), 129.4 (C-9), 131.1 (C-4), 147.4 (C-7). FT-IR (ATR. cm<sup>-1</sup>): 3359, 3105, 1599, 1427, 1255, 1089, 1026, 770, 729, 551. HR-MS mass calcd. for C<sub>13</sub>H<sub>11</sub>BrN<sub>2</sub>S 305.9826; found  $m/z$  305.9802.

#### 4.4.7. 2-Ethynyl-9H-fluorene (**7**)

In a 100 mL flask, 2-bromofluorene (2 g, 8.20 mmol) was dissolved in 40 mL of anhydrous THF, then, Pd(PPh<sub>3</sub>)<sub>2</sub>Cl<sub>2</sub> (0.29 g, 0.41 mmol) was added followed by CuI (78.1 mg, 0.41 mmol) and ethynyltrimethylsilane (3.47 mL, 24.59 mmol), finally *i*Pr<sub>2</sub>NH (2.31 mL, 16.39 mmol) was added slowly under constant bubbling of N<sub>2</sub>, the reaction was heated to 40 °C and maintained at that temperature overnight, the progress of the reaction was monitored by TLC and after the reaction was complete, the solvent was evaporated and the crude product was supported on celite. The compound was purified by flash chromatography with hexane, the deprotection of the silane was achieved by the reaction between the purified product **7** and K<sub>2</sub>CO<sub>3</sub>/CH<sub>3</sub>OH after the reaction was completed the solvent was evaporated and the reaction mixture was redissolved in dichloromethane and vacuum filtered, finally the solvent was evaporated to dryness to obtaining compound **7** as a light yellow solid in 88% (1.37g) yield. HR-MS mass calcd. for C<sub>15</sub>H<sub>10</sub> 190.0783; found  $m/z$  190.0768. Spectroscopic data of **7** agree with those previously reported.<sup>31</sup>

#### Acknowledgements

The authors thank CONACYT and PAPPIT IN 214513 for financial support. E.X.-F. (211329) thanks CONACYT for the PhD fellowship.

## Notes and References

<sup>a</sup> Facultad de Química, Departamento de Química Orgánica, <sup>b</sup> Departamento de Química Inorgánica y Nuclear, Universidad Nacional Autónoma de México, 04510, México, D. F., México. [Norberto.farfan@gmail.com](mailto:Norberto.farfan@gmail.com); [arturojs@cinvestav.mx](mailto:arturojs@cinvestav.mx)

<sup>c</sup> Departamento de Química de Biomacromoléculas, Instituto de Química, Universidad Nacional Autónoma de México, Circuito Exterior s/n, Ciudad Universitaria, 04510, México, D. F., México.

<sup>d</sup> Departamento de Química, Centro de Investigación y de Estudios Avanzados del IPN, Apdo. Postal 14-740, 07000, México, D. F., México.

† Electronic Supplementary Information (ESI) available: [NMR characterization and experimental procedures].

‡ These authors contributed equally.

1 Z. Yang, J. Cao, Y. He, J. H. Yang, T. Kim, X. Peng, J. S. Kim, *Chem. Soc. Rev.*, 2014, **43**, 4563-4601.

2 (a) M. A. Haidekker, E. A. Theodorakis, *J. Biol. Eng.*, 2010, **4**, 11. (b) M. A. Haidekker, T. P. Brady, D. Lichlyter, E. A. Theodorakis, *Bioorg. Chem.*, 2005, **33**, 415-425.

3 G. Deliconstantinos, V. Villiotou, J. C. Stavrides, *Biochem. Pharmacol.*, 1995, **49**, 1589-1600.

4 M. A. Haidekker, E. A. Theodorakis, *Org. Biomol. Chem.*, 2007, **5**, 1669-1678.

5 E. Lippert, W. Rettig, V. Bonacic-Koutecky, F. Heisel, J. A. Miehe, *Adv. Chem. Phys.*, 1987, **68**, 1-174.

6 (a) M. Baruah, W. Qin, R. A. L. Vallée, D. Beljonne, T. Rohand, W. Dehaen, N. Boens, *Org. Lett.*, 2005, **7**, 4377-4380. (b) A. B. Nepomnyashchii, A. J. Bard, *Acc. Chem. Res.*, 2012, **45**, 1844-1853.

7 (a) A. P. Demchenko, *J. Fluoresc.*, 2010, **20**, 1099-1128. (b) D. Dziuba, I. A. Karpenko, N. P. F. Barthes, B. Y. Michel, A. S. Klymchenko, R. Benhida, A. P. Demchenko, Y. Mély, A. Burger, *Chem. Eur. J.*, 2014, **20**, 1998-2009. (c) D. Fischer, E. A. Theodorakis, M. A.

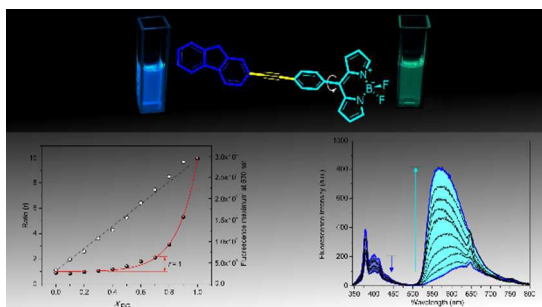
- Haidekker, *Nat. Protoc.*, 2007, **2**, 227-236. (d) M. A. Haidekker, T. P. Brady, D. Lichlyter, E. A. Theodorakis, *J. Am. Chem. Soc.*, 2006, **128**, 398-399.
- 8 K. Komatsu, Y. Urano, H. Kojima, T. Nagano, *J. Am. Chem. Soc.*, 2007, **129**, 13447-13454.
- 9 (a) A. P. de Silva, *Nat. Chem.*, 2012, **4**, 440-441. (b) M. T. Whited, N. M. Patel, S. T. Roberts, K. Allen, P. I. Djurovich, S. E. Bradforth, M. E. Thompson, *Chem. Commun.*, 2012, **48**, 284-286. (c) A. P. de Silva, H. Q. N. Gunaratne, T. Gunnlaugsson, A. J. M. Huxley, C. P. McCoy, J. T. Rademacher, T. E. Rice, *Chem. Rev.*, 1997, **97**, 1515-1566.
- 10 J. Rodríguez-Romero, L. Aparicio-Ixta, M. Rodríguez, G. Ramos-Ortíz, J. L. Maldonado, A. Jiménez-Sánchez, N. Farfán, R. Santillan, *Dyes Pigm.*, 2013, **98**, 31-41.
- 11 Z. Yang, Y. He, J.-H. Lee, N. Park, M. Suh, W.-S. Chae, J. Cao, X. Peng, H. Jung, C. Kang, J. S. Kim, *J. Am. Chem. Soc.*, 2013, **135**, 9181-9185.
- 12 M. A. Haidekker, T. P. Brady, D. Lichlyter, E. A. Theodorakis, *Bioorg. Chem.*, 2005, **33**, 415-425.
- 13 F. Fungo, L. A. Otero, L. Sereno, J. J. Silber, E. N. Durantini, *J. Mater. Chem.*, 2000, **10**, 645-650.
- 14 T. K. Khan, R. R. S. Pissurlenkar, M. S. Shaikh, M. Ravikanth, *J. Organomet. Chem.*, 2012, **697**, 65-73.
- 15 K. Y. Law, *Chem. Phys. Lett.* 1980, **75**, 545-549.
- 16 Th. Förster, G. Z. Hoffmann, *Phys. Chem.*, 1971, **75**, 63-76.
- 17 I. M. Smallwood, *Handbook Of Organics Solvent Properties*, Ed. John Wiley & Sons Inc., 1996.
- 18 B. Valeur, *Molecular Fluorescence*, Wiley-VCH, Weinheim, 2002.
- 19 H. Jin, M. Liang, S. Arzhantsev, X. Li, M. Maroncelli, *J. Phys. Chem. B*, 2010, **114**, 7565-7578.
- 20 (a) E. Lippert, *IUPAC Symposium on Hydrogen Bonding, Ljubljana*, 1957. (b) W. E. Acree Jr., D. C. Wilkins, S. A. Tucker, J. M. Griffin, J. R. Powell, *J. Phys. Chem.*, 1994, **98**, 2537-2544. (c) R. Królicki, W. Jarzęba, *J. Phys. Chem. A*, 2002, **106**, 1708-1713.
- 21 D. R. Lide, *CRC Handbook of Chemistry and Physics*, 2002; Ed. CRC Press.
- 22 J. Catalán, *J. Phys. Chem. B*, 2009, **113**, 5951-5960.



- 23 M. J. Kamlet, J. L. M. Abboud, M. H. Abraham, R.W. Taft, *J. Org. Chem.*, 1983, **48**, 2877-2887.
- 24 M. D. Bilokin, V. V. Shvadchak, D. A. Yushchenko, G. Duportail, Y. Mély, V. G. Pivovarenko, *J. Fluoresc.*, 2009, **19**, 545-553.
- 25 R. L. Martin, *J. Chem. Phys.*, 2003, **118**, 4775-4777.
- 26 (a) E. Bahaidarah, A. Harriman, P. Stachelek, S. Rihn, E. Heyer, R. Ziessel, *Photochem. Photobiol. Sci.*, 2014, **13**, 1397-1401. (b) G. Ulrich, R. Ziessel, A. Harriman, *Angew. Chem., Int. Ed.*, 2008, **47**, 1184-1201. (c) A. C. Benniston, A. Harriman, V. L. Whittle M. Zelzer, *Eur. J. Org. Chem.*, 2010, 523-530.
- 27 T. L. Bahers, C. Adamo, I. Ciofini, *J. Chem. Theory Comput.*, 2011, **7**, 2498-2506.
- 28 S. Fery-Forgues, D. Lavabre, *J. Chem. Educ.*, 1999, **76**, 1260-1264.
- 29 (a) C. Amovilli, V. Barone, R. Cammi, E. Cancès, M. Cossi, B. Mennucci, C. S. Pomelli, J. Tomasi, *Adv. Quant. Chem.*, 1998, **32**, 227-261. (b) J. Tomasi, B. Mennucci, R. Cammi, *Chem. Rev.*, 2005, **105**, 2999-3094.
- 30 Gaussian 09, Revision **D.01**, M. J. Frisch, G. W. Trucks, H. B. Schlegel, G. E. Scuseria, M. A. Robb, J. R. Cheeseman, G. Scalmani, V. Barone, B. Mennucci, G. A. Petersson, H. Nakatsuji, M. Caricato, X. Li, H. P. Hratchian, A. F. Izmaylov, J. Bloino, G. Zheng, J. L. Sonnenberg, M. Hada, M. Ehara, K. Toyota, R. Fukuda, J. Hasegawa, M. Ishida, T. Nakajima, Y. Honda, O. Kitao, H. Nakai, T. Vreven, J. A. Montgomery, Jr., J. E. Peralta, F. Ogliaro, M. Bearpark, J. J. Heyd, E. Brothers, K. N. Kudin, V. N. Staroverov, R. Kobayashi, J. Normand, K. Raghavachari, A. Rendell, J. C. Burant, S. S. Iyengar, J. Tomasi, M. Cossi, N. Rega, J. M. Millam, M. Klene, J. E. Knox, J. B. Cross, V. Bakken, C. Adamo, J. Jaramillo, R. Gomperts, R. E. Stratmann, O. Yazyev, A. J. Austin, R. Cammi, C. Pomelli, J. W. Ochterski, R. L. Martin, K. Morokuma, V. G. Zakrzewski, G. A. Voth, P. Salvador, J. J. Dannenberg, S. Dapprich, A. D. Daniels, Ö. Farkas, J. B. Foresman, J. V. Ortiz, J. Cioslowski, D. J. Fox, Gaussian, Inc., Wallingford CT, 2009.
- 31 (a) E. Lager, J. Liu, A. Aguilar-Aguilar, B. Z. Tang, E. Peña-Cabrera, *J. Org. Chem.*, 2009, **74**, 2053-2058. (b) Y. Fu, Q. He, D. Zhu, Y. Wang, Y. Gao, H. Cao, J. Cheng., *Chem. Commun.*, 2013, **49**, 11266-11268.



## Table of Contents Graphic



Two fluorescent ratiometric fluorene derived Bodipy probes present a sensitive response to microviscosity changes.